MICROBIOLOGY

Phospholipid distribution in the cytoplasmic membrane of Gram-negative bacteria is highly asymmetric, dynamic, and cell shape-dependent

Mikhail Bogdanov[1,2]*, Kyrylo Pyrshev[1,3,4], Semen Yesylevskyy[4,5], Sergey Ryabichko[1,6], Vitalii Boiko[1,7], Pavlo Ivanchenko[1,8], Ramziya Kiyamova[2], Ziqiang Guan[9], Christophe Ramseyer[5], William Dowhan[1]

The distribution of phospholipids across the inner membrane (IM) of Gram-negative bacteria is unknown. We demonstrate that the IMs of *Escherichia coli* and *Yersinia pseudotuberculosis* are asymmetric, with a 75%/25% (cytoplasmic/periplasmic leaflet) distribution of phosphatidylethanolamine (PE) in rod-shaped cells and an opposite distribution in *E. coli* filamentous cells. In initially filamentous PE-lacking *E. coli* cells, nascent PE appears first in the periplasmic leaflet. As the total PE content increases from nearly zero to 75%, cells progressively adopt a rod shape and PE appears in the cytoplasmic leaflet of the IM. The redistribution of PE influences the distribution of the other lipids between the leaflets. This correlates with the tendency of PE and cardiolipin to regulate antagonistically lipid order of the bilayer. The results suggest that PE asymmetry is metabolically controlled to balance temporally the net rates of synthesis and translocation, satisfy envelope growth capacity, and adjust bilayer chemical and physical properties.

INTRODUCTION

The asymmetric transmembrane distribution of individual lipids in biological membranes is a ubiquitous feature of most, if not all, biological membranes (*1*). The maintenance of this asymmetry and controlled distribution of lipids across various cell membranes plays a pivotal role in cellular life and death. Loss or alteration of lipid asymmetry is reportedly linked to the processes of apoptosis (*2*), oncogenesis (*3*), and cell division (*2*). However, we are still far from fully understanding the physiological significance and detailed molecular mechanisms by which membrane phospholipid asymmetry is generated, maintained, and modulated (*1*). Particularly, the role of lipid asymmetry in bacteria is much less studied than in eukaryotic cells (*4*).

Because of its zwitterionic nature at physiological pH and unique structural physical properties, phosphatidylethanolamine (PE) is associated with a number of cellular activities. It modulates lipid bilayer spontaneous curvature (*4*), acts as a lipochaperone (*5*), provides a net neutral charge to support membrane protein topogenesis (*6*, *7*), supports the activity of several respiratory complexes (*8*), and participates in the transport of fully folded proteins across bacterial membranes (*9*). A cycle of PE externalization followed by internalization is essential during cell division in the cells of lower and higher eukaryotes (*2*). PE is the major phospholipid in Gram-negative bacteria and the second most abundant phospholipid in mammalian cells. PE comprises about 75% of the phospholipid in the cell envelope of *Escherichia coli* and other Gram-negative bacteria. Inner membrane (IM) PE content is roughly 50% given the high PE content of the inner leaflet of outer membrane (OM) bilayer (*10*).

PE is enriched in the inner leaflet of mammalian plasma membranes (*11*), the cell membrane of *Bacillus subtilis* (*12*), and the OM of *E. coli*. However, its distribution within the IM of Gram-negative bacteria is still unknown (*4*). The complex double-membrane organization of the cell envelope in Gram-negative bacteria places unique biosynthetic and topological constraints on PE distribution, which can affect transmembrane distribution of newly synthesized and steady-state PE within the IM.

Whether and how *E. coli* can maintain a lipid asymmetry (biosynthetically, physically, or enzymatically) is still unknown. No specific flippases or scramblases have been identified in the biogenic IM of *E. coli*. Nevertheless, from a structural, topological, and thermodynamic view, PE is expected to be localized within the concave cytoplasmic leaflet of membranes (*4*, *13*). Synthesis of PE begins by formation of phosphatidylserine (PS) by a synthase localized to the cytoplasmic surface of the IM, followed by conversion to PE by the IM integral PS decarboxylase (Psd) (*10*). However, from a biosynthetic view, a pool of PE should be continuously available within the periplasmic surface of the IM to serve as an ethanolamine or acyl donor for the continuous modification of newly synthesized lipid A or the N terminus of OM lipoproteins in stressed and both stressed and resting Gram-negative bacteria, respectively (*14*). In addition, PE must continuously flow from the outer leaflet of the IM to the periplasmic leaflet of the OM during cell growth.

The localization and dynamics of this important phospholipid could be characterized by vectorial molecular probes. In this work, we use 2,4,6-trinitrobenzenesulfonic acid (TNBS) that does not readily

[1]Department of Biochemistry and Molecular Biology, McGovern Medical School at The University of Texas Health Science Center at Houston, TX 77030, USA. [2]Department of Biochemistry, Biotechnology and Pharmacology, Kazan Federal University, Institute of Fundamental Medicine and Biology, Kazan 420008, Russian Federation. [3]Laboratory of the Nanobiotechnology, Department of Neurochemistry, Palladin Institute of Biochemistry of the NAS of Ukraine, 9 Leontovycha Street, Kyiv 01601, Ukraine. [4]Department of Physics of Biological Systems, Institute of Physics, NAS of Ukraine, 46 Nauky Avenue., Kyiv 03680, Ukraine. [5]Laboratoire Chrono-Environnement UMR CNRS 6249, Université de Bourgogne Franche-Comté, 16 route de Gray, 25030 Besançon Cedex, France. [6]Lewis-Sigler Institute for Integrative Genomics, Princeton University, Princeton, NJ 08540, USA. [7]Department of Spectroscopy of Excited States, Institute of Low Temperature and Structure Research, Polish Academy of Sciences, Okólna 2, Wrocław 50-422, Poland. [8]Department of Chemistry and Interdepartmental Centre Nanostructured Interfaces and Surfaces (NIS), University of Torino, 10125 Torino, Italy. [9]Department of Biochemistry, Duke University Medical Center, Durham, NC 27710, USA.
*Corresponding author. Email: mikhail.v.bogdanov@uth.tmc.edu

penetrate biological or liposomal membranes and has been used to determine aminophospholipid transmembrane distributions in bacterial (*12*, *15*) and mammalian cells (*16*, *17*). In contrast, 1,5-difluoro-2,4-dinitobenzene (DFDNB) labels free amine groups of lipids in both membrane leaflets due to its high permeability (*18*, *19*). However this reagent has not been used extensively to label free amine groups of lipids. Since Gram-negative bacteria have a complex envelope system of IMs and OMs, we used uniformly oriented inside out membrane vesicles (ISOv), which are fully devoid of OMs. Combination of TNBS and DFDNB probes allowed us to confidently assess PE asymmetry in the IM of Gram-negative bacteria. The assay determines the pool of PE that is either fully accessible to or protected from the reaction with DFDNB or TNBS, respectively.

In addition, our assay allowed us to address a long-standing question in biology of how bacterial cells control their size. While recent studies have focused on protein-centric mechanisms (*20*), we addressed the role of lipid composition and transmembrane lipid dynamics in the regulation of the cell size and shape of *E. coli*. Present study provides the first direct evidence that PE predominates in the cytoplasmic leaflet of the IM of wild-type *E. coli* with an opposite distribution in filamentous cells. We extended this study to ISOv made from genetically altered "lipid mutants" with different amounts of PE, PS, or cardiolipin (CL). Counterintuitively and unexpectedly, newly synthesized PE first appears in the outer leaflet of the IM, followed by movement to the inner leaflet or continuous biosynthetic buildup in the inner leaflet. Moreover our results support the existence of tight regulation of PE transmembrane distribution and CL content to maintain a bilayer packing order and propensity toward asymmetric distribution of PE in the IM of *E. coli*.

In this work, we were also able to lock transmembrane PE fluxes at different stages of cell morphogenesis in pulse-chase experiments in wild-type and filamentous *E. coli* by taking advantage of the strains in which PE can be eliminated, tightly titrated, or controlled temporally. We reveal that PE distribution across the IM of *E. coli* is asymmetric, dynamic, cell shape–dependent and likely regulated via metabolic control, biosynthetic (anabolic and catabolic) demands and physical and topological constraints to coordinate and balance envelope growth and capacity.

RESULTS

Experimental rationale

In ISOv, the external and luminal surfaces correspond topologically to the cytoplasmic and periplasmic leaflets, respectively, of the IM of whole cells (Fig. 1A). Several independent approaches were used to establish phospholipid asymmetry of the *E. coli* IM. To selectively

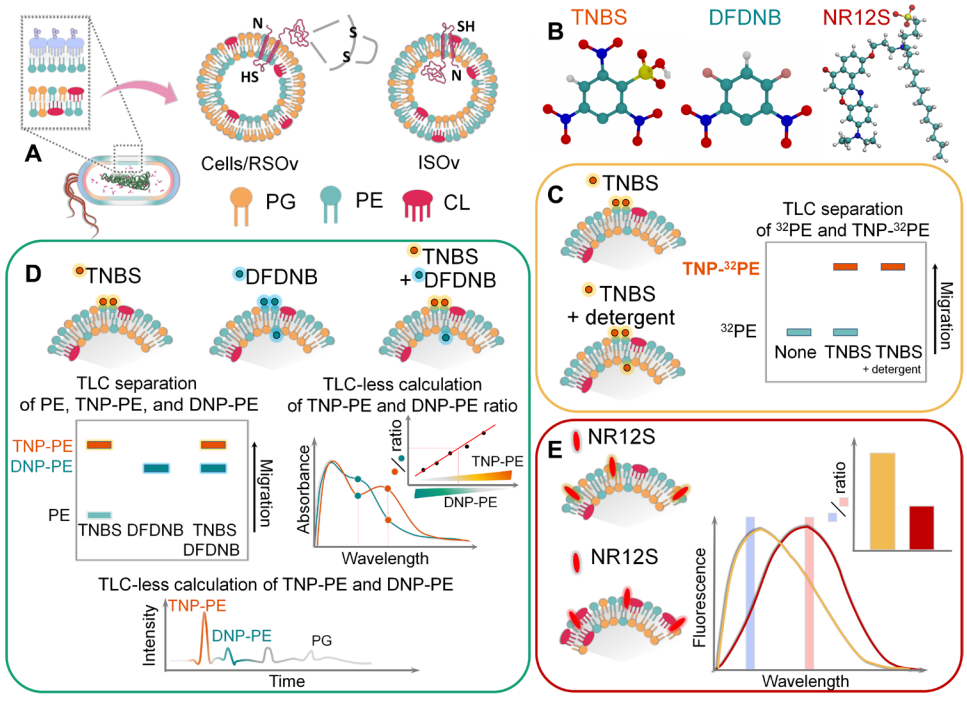

Fig. 1. Rationale for the development of aminophospholipid compositional and physical lipid asymmetry assays for ISOv using amino-reactive probes and leaflet-specific probe for lipid order. (**A**) In contrast to whole cells and right side out IM vesicles (RSOv), the outer leaflet of ISOv derived from the IM of *E. coli* corresponds topologically to the cytoplasmic side of the IM. ISOv are uniformly oriented and fully devoid of OMs. The transmembrane orientation of *E. coli* leader peptidase (LepB) (see the main text and Fig. 2D) was used to verify the sidedness of isolated ISOv. LepB embedded in the *E. coli* IM is shown. (**B**) Chemical structures of membrane nonpermeant TNBS and permeant DFDNB and outer leaflet–specific NR12S. (**C**) TLC-based PE sidedness assay. TLC-resolved derivatized aminophospholipids were used to calculate the percentage of the ^{32}P-labeled PE pool that is either protected from or accessible to reaction with nonpermeant TNBS in the presence or absence of detergent. (**D**) Spectrophotometric TLC elution–based and TLC-less aminophospholipid sidedness assays. After separate or sequential treatment with TNBS and DFDNB, the percentage of PE in each IM leaflet was estimated from the measurement of maximum absorbance of TLC-separated and eluted trinitrophenol-PE (TNP-PE) and dinitrophenyl–PE (DNP-PE). Alternatively, amounts of TNP-PE and DNP-PE were determined by normal-phase LC/MS/MS (liquid chromatography–tandem mass spectrometry) or by measurement of the absorption spectrum of total chloroform extracts at wavelengths corresponding to absorption maxima of TNP-PE and DNP-PE. (**E**) Monitoring of lipid order in outer leaflet by Nile red–based NR12S fluorescent probe whose structure precludes transbilayer flip-flop. This dye localizes exclusively within the outer leaflet of model and biological membranes and exhibits a red shift in liquid-disordered phase.

label aminophospholipids within the inner and outer leaflet of the IM, we used two probes (Fig. 1B) with different membrane-penetrating and chemical properties to establish the transmembrane distribution of PE and PS in ISOv. Lipid derivatives were quantified using radiometric, spectrophotometric, or mass spectrometric methods with and without separation of derivatives by thin-layer chromatography (TLC) (Fig. 1, C and D). TNBS does not cross lipid bilayers of bacterial and mammalian cells, organelles, or liposomes because of its water solubility and net negative charge (*12*, *17*). However, DFDNB does cross lipid bilayers because of its electroneutrality and solubility in dimethyl sulfoxide (DMSO) (*18*, *19*). The Nile red–based NR12S fluorescent probe localizes exclusively in the outer leaflet of biological membranes and distinguishes liquid ordered (L_o) from liquid disordered (L_d) phases (Fig. 1, B and E) (*21*). It was expected that a variety of different rigidity/hydration states within the L_d phase will be observed in the leaflets of *E. coli* ISOv, which cannot form L_o phase without cholesterol.

Sidedness of PE in ^{32}P-labeled ISOv isolated from wild-type *E. coli* cells

Sidedness of PE was estimated from the amount of radiolabeled PE and its derivatized product [trinitrophenyl-PE (TNP-PE)] obtained after TNBS treatment of intact and octyl glucoside (OG) solubilized uniformly oriented ISOv isolated from ^{32}P-labeled cells (Figs. 1C and 2A). ISOv were free of OM contamination, as evidenced by Western blots of subcellular marker proteins for an OM (PldA) and IM (SecA) protein (Fig. 2C). Orientation of *E. coli* leader peptidase (LepB) (Fig. 1A) was used to verify the sidedness of isolated ISOv as previously described (*6*). The percentage (98%) of IM vesicles that adapted an ISO orientation was determined by the substituted-cysteine accessibility method as applied to transmembrane domain orientation (SCAM) (Fig. 2D). Membrane impermeable and avidin–horseradish peroxidase detectable biotinylated 3-(*N*-maleimidylpropionyl) biocytin (MPB) and nonpermeant transparent 4-acetamido-4′-maleimidylstilbene-2,2′-disulfonic acid (AMS) sulfhydryl reagents were used to probe the sidedness of extramembrane domains of *E. coli* LepB, which was used as an essential model protein not sensitive to changes in lipid composition or cell morphology (*6*). LepB has one reduced and therefore fully reactive Cys residue exposed to the cytoplasm and located outside of ISOv with its external surface topologically corresponding to the cytoplasmic leaflet (Fig. 1A). The two "silent" Cys's in disulfide linkage exposed to the periplasm should be accessible from the lumen of ISOv only after OG solubilization and reduction with β-mercaptoethanol (βME). Therefore, in intact ISOv blocking with AMS only occurs with the solvent-accessible and surface-exposed Cys. Thus, ISOvs were either labeled directly with MPB or first pretreated with AMS, followed by treatment with MPB in the absence or presence of detergent OG or by MPB in the presence of OG and βME. Labeling by MPB that can be blocked completely by pretreatment with AMS is an independent indication of an outward-facing residue and inside out orientation of ISOv, while the labeling by MPB that cannot be blocked by AMS treatment is an independent indication of a residue that faces the lumen of ISOv.

The optimal conditions for determination of the accessibility of PE to TNBS were established by incubating wild-type *E. coli* ISOv with different concentrations of TNBS for different times and temperatures. The amount of PE that reacted with TNBS did not increase at concentrations above 1 mM, indicating that TNBS was able to label all the surface-accessible amino groups under the indicated

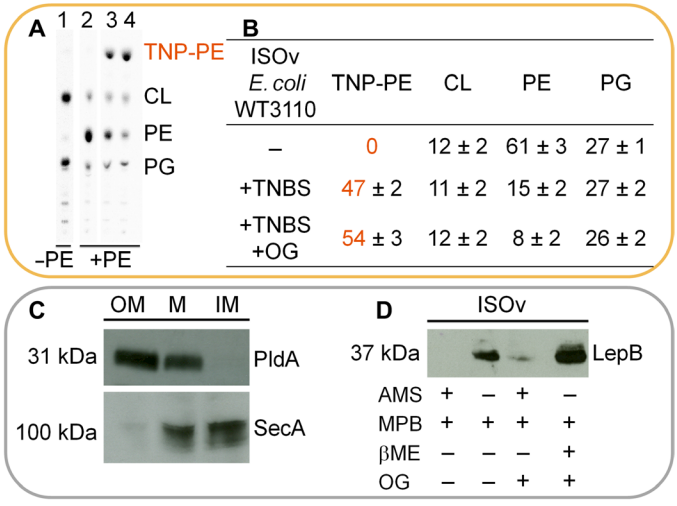

Fig. 2. The labeling of *E. coli* ^{32}P-labeled ISOv with TNBS to assess transmembrane distribution of PE. (**A**) ISOv prepared from exponentially grown PE-lacking (AL95) or wild-type (W3110) *E. coli* uniformly labeled with [^{32}P]PO_4 were labeled with TNBS. Conditions for TNBS treatment: PE-lacking cells, lane 1, and 1 mM at 4°C/1 hour. Trace spot (0.3 to 0.5%) with PE mobility corresponds to undecaprenyl phosphate (C55-P) (*30*). Wild-type, lane 2, none; lane 3, 1 mM at 4°C/1 hour; lane 4, 1 mM at 37°C/1 hour in the presence of OG. Reactions were quenched; the total phospholipids were isolated, separated by TLC, and quantified with a Personal Molecular Imager FX as described in Materials and Methods. (**B**) Distribution of ^{32}P-labeled PE between the inner and outer leaflet. The amount of PE was calculated from amounts of ^{32}P-labeled PE and TNP-PE expressed as mole percent (mol %) of total aminophospholipid (PE + TNP-PE) content after subtraction of the amount of PE nonderivatized even in the presence of detergent. Results in sequential rows are from lanes 2, 3, and 4, respectively. Values (mol %) are means (±SD) from three experiments, where each determination was performed in duplicate. Variation between duplicates was ±3% of the mol % values. (**C**) An isopycnic sucrose gradient of cells disrupted as described in Materials and Methods was fractionated, and fractions with different buoyant densities corresponding to OM, a mix (M) of both (IM + OM) and IM were analyzed by SDS–polyacrylamide gel electrophoresis (SDS-PAGE) and Western blotting using antibody against subcellular marker proteins for the OM (PldA) and IM (SecA). (**D**) Nearly 100% ISOv were prepared from exponentially grown wild-type of *E. coli*, treated as indicated and subjected to SDS-PAGE and Western blotting using avidin–horseradish peroxidase. A total of 98% of LepB reacted with MPB and biotinylation was prevented by prior treatment with AMS. About 2 to 3% of reactivity not blocked by prior addition of AMS in OG solubilized vesicles results from either lysed vesicles or vesicles with RSO (Fig. 1A) orientation. Solubilization with OG and reduction of the disulfide linkage with βME led to labeling of all reduced cysteines.

experimental conditions such that the reaction reaches saturation of available primary amines. Upon TNBS treatment, a new spot appeared on TLC, which was identified by mass spectrometry as TNP-PE (Fig. 2A, lane 3). This spot was not present after treatment of ISOv made from PE-lacking cells (Fig. 2A, lane 1), demonstrating the specificity of TNBS. The distribution of PE in periplasmic and cytoplasmic leaflets of the IM was calculated from the proportion of maximally accessible PE after solubilization of the ISOv with OG (Fig. 2B). In the absence of detergent, PE was only partially (77%) converted into TNP-PE (Fig. 2A, lane 3). Treatment of solubilized ISOv with TNBS resulted in another 11% of PE converted into TNP-PE (Fig. 2A, lane 4). Although the sum of the radioactivity in the PE and TNP-PE spots remains nearly constant in both cases (Fig. 2A, lanes 3 and 4), the conversion of PE into the TNBS derivative was not complete in the presence of detergent. The failure to obtain

complete labeling of PE in solubilized membranes might be explained by clustering of this lipid around proteins, phase separation, or spatial restrictions due to the introduction of this reagent or both events (*17*). Despite the fact that 13% of PE was still inaccessible after OG treatment, 75 to 80% of total PE was labeled in ISOv with TNBS (corresponding to the inner leaflet of the IM), and the remaining 20 to 25% was not accessible to the reagent with about half of that definitely in the outer leaflet of the IM (Fig. 2B). As discussed below with respect to reactivity of PE in liposomes (fig. S7), the unreactive PE in ISOv appears to be due to tight interaction with proteins in agreement with published results (*22*). Nevertheless, the IM of *E. coli* is asymmetric with approximately 75% of the PE in the cytoplasmic leaflet. Although the amount of total PE in the IM of wild-type *E. coli* was previously estimated from pulse [^{32}P]PO_4 radiolabeling (*10*), our relevant results from steady-state labeling indicate 61 ± 3% of PE in the IM.

Spectrophotometric TLC elution–based PE topography assay

Impermeable TNBS was combined with DFDNB, which can freely penetrate through lipid bilayers (Fig. 1, B and D). To determine a maximal pool of PE in ISOv and check whether the added amount of DFDNB was sufficient to convert the entire pool of PE present in the vesicles, DFDNB was added to vesicles solubilized with OG. Figure 3A (lanes 3 and 4) shows that the conversion of PE into the dinitrophenyl–PE (DNP-PE) derivative was complete in either the absence or presence of detergent. Moreover DNP-PE runs slower than TNP-PE (Fig. 3A, lanes 2 to 4) on TLC, suggesting that both reagents can be used sequentially to determine sidedness of PE without a detergent treatment (Fig. 3A, lane 5). As shown in Fig. 3A, PE was the only lipid that reacted with TNBS and DFDNB, and the PE spot disappeared with a concomitant appearance of either TNP-PE or DNP-PE (lanes 2 and 3) or both derivatives (lane 5) if ISOv were treated separately or sequentially with these reagents. When TNP-PE or DNP-PE was eluted from the TLC plates and quantified on the basis of their absorbance maximum at 337 nm, separate (lanes 2 and 4) and sequential (lane 5) labeling gave essentially the same amount of protected PE (25%) located in the luminal leaflet of ISOv, confirming that all surface-accessible PE molecules were labeled by TNBS, and the fraction of PE that was not available to TNBS but available to DFDNB is the same set of molecules. Thus, no normalization per amount of phospholipid or protein is required, and lipid asymmetry can be assessed by determining lipid pools, which are labeled with TNBS and fully accessible to subsequent reaction with DFDNB.

Only monosubstituted products of PE were observed after DFDNB treatment (Fig. 3A, lanes 3 to 5). The absence of disubstituted products, i.e., replacement of both fluorines by ethanolamine, was observed previously (*18*, *23*). It was suggested that the inability of DFDNB to cross-link PE molecules can be attributed to location of PE molecules in protein complexes at the inner surface of the erythrocyte or microsomal membranes rather than in the phospholipid bilayer (*22*), the faster reaction of the head group primary amine with the first fluorine atom (*18*), or short distance between the two reactive fluorine

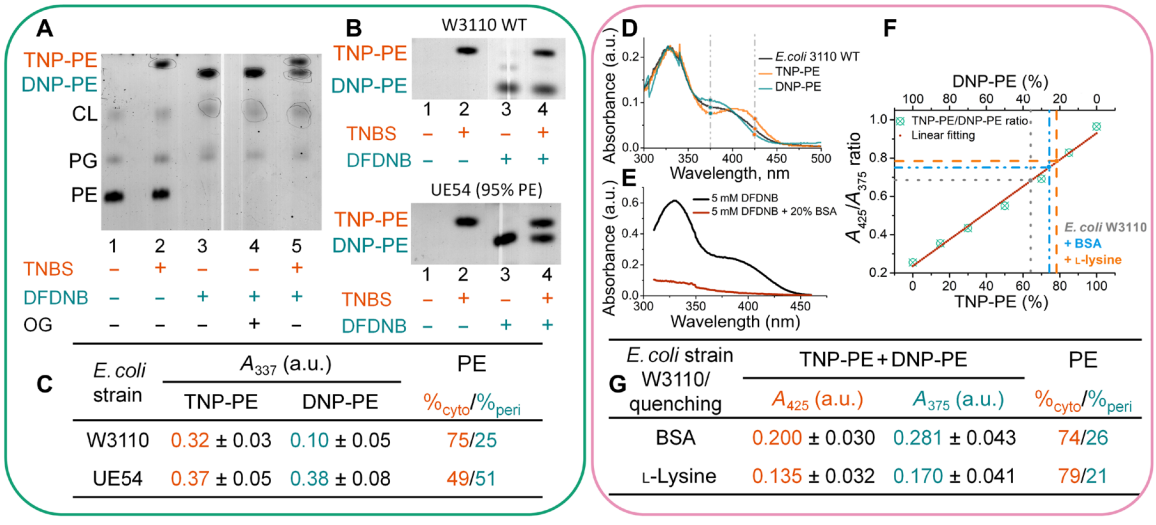

Fig. 3. Spectrophotometric TLC elution and TLC-less PE topography assays. (**A**) ISOv were separately or sequentially treated with TNBS/DFDNB, followed by TLC separation of TNP-PE and DNP-PE, elution of derivatives, and quantification by maximum absorbance. TLC of derivatized and nonderivatized phospholipids from wild-type ISOv was visualized by exposure to iodine. Samples were untreated (lane 1), treated separately (lanes 2 to 4), or sequentially with TNBS followed by DFDNB (lane 5). (**B**) TLC of derivatized PE in ISOv derived from *E. coli* wild-type (W3110) or the UE54 mutant [lacking phosphatidylglycerol (PG) and CL] either untreated (lane 1) or treated separately (lanes 2 and 3) or sequentially (lane 4) with TNBS and DFDNB, respectively. (**C**) TNP-PE and DNP-PE spots, representing PE from the outer and inner leaflets of the ISOv, respectively, were eluted from the TLC plates and quantified on the basis of their absorbance maximum at 337 nm (D). The values are represented as average absorbances (±SD) of TNP-PE and DNP-PE from three separately isolated ISOv preparations. The final ratiometric calculation of the percent distribution of PE between the inner and outer leaflet (far right column) varied by ±5% of the percent values. a.u., arbitrary units. (**D**) Scanning absorbance spectra of isolated TNP-PE or DNP-PE and a total chloroform extract of ISOv treated sequentially with TNBS followed by DFDNB. (**E**) A scanning absorbance spectra of mock chloroform extract of buffer containing 5 mM DFDNB prepared before and after termination of labeling by bovine serum albumin (BSA). (**F**) Eluted TNP-PE and DNP-PE spots were mixed in different proportions; the absorbance was measured at 425 and 375 nm, and the A_{425}/A_{375} ratios were plotted as a function of the mole fraction of each derivative to generate a standard curve. (**G**) Total lipids were extracted from ISOv labeled sequentially with TNBS followed by DFDNB and quenched with BSA or L-lysine. The amount of PE in the outer and inner leaflets was determined after calculating the A_{425}/A_{375} ratio using the standard curve in (F), which normalizes for the different observed absorbances for the BSA and lysine samples that contained different amounts of protein. Estimated amount of TNP-PE and DNP-PE from measurement of the total lipid extract of ISOv sequentially labeled with TNBS, followed by DFDNB and quenched either with BSA (blue dashed line) or L-lysine (orange dashed line) in (F). The variability in the final percent distribution was the same as in (C).

atoms (*23*). To distinguish between these possibilities and to elucidate the monofunctional cross-linking mechanism, we performed ab initio quantum chemistry calculations of corresponding reactions and all-atom molecular dynamics simulations of lipid bilayers containing a mixture of monosubstituted FDNB-PE and PE. Potential energy scanning of reaction coordinates for substitution of the first and second fluorine demonstrated that the optimal distance between the reacting carbon and nitrogen is about 2.2 Å, supporting a steric exclusion mechanism. Moreover, substitution of the second fluorine in the FDNB-PE derivative, despite being thermodynamically favorable, does not happen in lipid bilayers due to the very short lifetime of the close pairs of reacting atoms (see the Supplementary Materials).

TNP-PE absorption is linearly proportional to its concentration (*16*) in organic solvent. The absorption maximum of isolated TNP-PE and DNP-PE is 337 nm (Fig. 3D). Since different chromogenic probes are used to reveal an asymmetric distribution of aminophospholipids, it is important to know whether the derivatives have the same molar extinction coefficients. The molar extinction coefficients of TNP-PE, TNP-PS, and DNP-derivatives at their optimal wavelengths were essentially the same (17140 ± 750), confirming that different species within one lipid class have the same extinction coefficient (*24*). Thus, absorbance of TNP-PE can be directly compared to DNP-PE as a function of the derivatized amount of PE. TNP-PE and DNP-PE spots, representing PE in the outer and inner leaflets of ISOv, respectively, can be eluted, and the amount of DNP-PE and TNP-PE can be quantified based on absorbance at 337 nm. Although the absolute absorbance at 337 nm varies with the amount of lipid in each sample (thus, the high variability among samples in Fig. 3D), the ratio of absorbances [$A_{\text{DNP-PE}}$] or [$A_{\text{TNP-PE}}$] to [$A_{\text{DNP-PE}} + A_{\text{TNP-PE}}$] is independent of the lipid and protein content of ISOv. Therefore, using a ratiometric approach eliminates the need for normalization of absorption values of TNP and DNP derivatives, and lipid sidedness is directly correlated with these ratios. The amounts of PE present within the external and internal leaflets of ISOv isolated from wild-type strain W3110 estimated from independent (Fig. 3B, lanes 2 and 3) or sequential labeling (lane 4) were essentially the same and were averaged in Fig. 3C. In ISOv made from wild-type cells, 75% (cytoplasmic) of PE was trinitrophenylated and only 25% (periplasmic) was dinitrophenylated, e.g., fully accessible to subsequent reaction with DFDNB. Therefore, these results are consistent with our previous results (Fig. 2, A and B) using radiolabeled phospholipids and TNBS alone. ISOv made from *Yersinia pseudotuberculosis* (*Yptb*) exhibit the same disproportionality in PE distribution (fig. S4).

To further validate the sidedness assay, we isolated ISOv from the mutant UE54 strain containing about 95% of its phospholipid as PE (*25*). PE would be expected to be uniformly distributed across the IM consisting of 80% PE (fig. S5). For this strain, the same amount (49 to 50%) was protected from TNBS and derivatized by subsequent treatment with DFDNB consistent with uniform distribution of PE in the IM of these cells (Fig. 3, B and C).

Although the amount of total PE in the IM was previously estimated from pulse [^{32}P]PO_4 radiolabeling (*10*), our own result are shown in fig. S5 where the amount of PE was calculated in IMs isolated from uniformly labeled [^{32}P]PO_4 radiolabeled cells. The amount of PE in IM of wild-type and different *E. coli* mutants varied from near 60 to 80% in phosphatidylglycerol (PG) and CL, lacking UE54 strain but never exceeding the amounts virtually allowed in each leaflet.

TLC-less determination of PE sidedness in ISOv

A scanning spectrum of isolated TNP-PE and DNP-PE demonstrates that these PE derivatives have characteristic and distinguishable spectra (Fig. 3D). Although absorption maximum peaks exist in the region of 337 to 340 nm, the absorption curves of TNP-PE and DNP-PE form specific shoulders at 425 and 375 nm, respectively. Since the ratio of A_{425}/A_{375} linearly increases with increasing ratio of TNP-PE/DNP-PE (Fig. 3F), the amount of PE in outer and inner leaflets of ISOv can be calculated from this ratio determined in a chloroform extract of ISOv after treatment with TNBS, followed by DFDNB without TLC extraction or normalization.

Since DMSO-soluble DFDNB is coextracted with TNP-PE and DNP-PE in the TLC-less aminophospholipid sidedness assay, the sequential treatment of ISOv with TNBS and DFDNB was terminated by bovine serum albumin (BSA) or L-lysine to inactivate and scavenge unreacted TNBS and DFDNB. Derivatized lipids were extracted, leaving the inactive amino-specific labels at the interphase formed after the two-phase extraction procedure (Fig. 3E). When TNBS and DFDNB-labeled lipids were analyzed after elution from TLC (Fig. 3C) or directly in chloroform extracts (Fig. 3, F and G) after quenching of labeling with either BSA or L-lysine, essentially the same percentage of TNP-PE and DNP-PE corresponding to PE in outer and luminal leaflets of ISOv, respectively, was obtained (Fig. 3G). Therefore, the IM of wild-type cells is asymmetric with an approximate 75%/25% (cytoplasmic/periplasmic) distribution of PE in accordance with results of both the TLC elution–based and TLC-less assays.

The nonbilayer prone nature of negatively curved PE species increases with unsaturated fatty acid content, which might favor localization of unsaturated fatty acid species of PE to the cytoplasmic leaflet of the IM resulting in PE acyl group asymmetry. Therefore, we subjected TLC-eluted TNP-PE and DNP-PE from ISOv of wild-type strain W3110 labeled sequentially with TNBS followed by DFDNB to mass spectral analysis. The predominate PE species in both cases was 16:0/16:1, indicating no difference in the fatty acid composition in either leaflet of the IM (fig. S6).

PS distribution in the IM of *E. coli*

Normally, PS is present only in trace amounts in *E. coli* since it is immediately converted to PE by the integral membrane enzyme PS decarboxylase to PE (*26*). However, the conditional lethal thermosensitive mutant (*psd*^{ts}) EH150, when grown the presence of Mg^{2+} (suppresses lethal effect of low PE) at the nonpermissive temperature of 42°C, accumulates PS at levels above 10 to 20% of total phospholipid at the expense of PE (*26*). PS at steady state distributes equally between the IM and OM (*10*). PS differs from PE in that it is negatively charged at neutral pH. Since this strain accumulated two other negatively charge phospholipids, PG and CL, the cells could adjust electrostatic charge balance across the membrane by regulating their distribution across the IM (*10*). Therefore, we assessed PS transmembrane distribution in ISOv made from EH150 grown at the nonpermissive temperature in the presence of 25 mM $MgCl_2$.

The mobility of TNP and DNP derivatives of PS and PE in a TLC system was confirmed by derivatization of commercial PE and PS (Fig. 4A). Notably, we found that PE exhibits 44%/66% (cytoplasmic/periplasmic) distribution, while PS was not accessible to reaction with TNBS but was fully derivatized by DFDNB (Fig. 4, B and C), consistent with 96% of PS localized to the periplasmic leaflet. Although PE was found to react more rapidly than PS within the first 20 min (*16*),

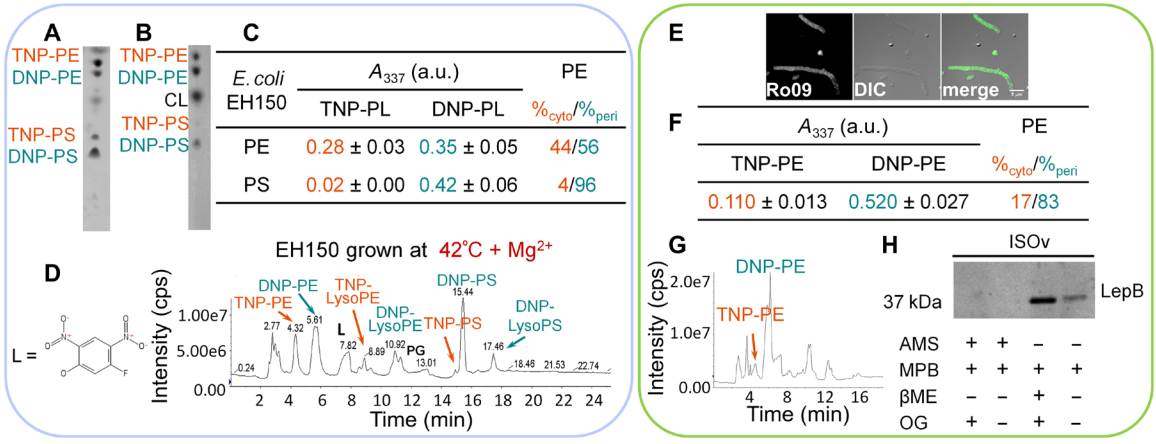

Fig. 4. Transbilayer distribution of PS and PE in ISOv prepared from the *E. coli psd* mutant. (**A**) TLC of TNBS- and DFDNB-labeled liposomal PE and PS visualized by iodine contrast. (**B**) TLC with derivatized phospholipids from ISOv treated sequentially with TNBS followed by DFDNB. (**C**) TNP and DNP phospholipid (PL) derivatives eluted from the TLC (B) and quantified by their absorbance at 337 nm. The percentage of TNP to DNP aminophospholipid derivatives was used as index of outer-to-inner leaflet phospholipid asymmetry. The values are represented as average absorbances (±SD) of TNP and DNP aminophospholipids from three separately isolated ISOv preparations. The final ratiometric calculation of the percent distribution between the inner and outer leaflet (far right column) varied by ±3% or less of the percent values. (**D**) Normal-phase LC/MS/MS analysis of DNP-PE and TNP-PE and DNP-PS and TNP-PS in total lipid extract of ISOv treated sequentially with TNBS followed by DFDNB. L corresponds to DFDNB. (**E**) Transbilayer distribution of PE in ISOv prepared from filamentous *E. coli* cells containing 63% of IM PE. Aztreonam-treated cells harvested and processed to visualize PE content by fluorescent microscopy as described in Materials and Methods. Fluorescence and DIC (differential interference contrast) images are shown. (**F**) Determination of the distribution of PE in ISOv assayed by the TLC elution–based method. Values are average absorbances (±SD) and calculated distribution from three experiments, where each determination was performed in duplicate with similar variance as described in (C). (**G**) Normal-phase LC/MS/MS analysis of DNP-PE and TNP-PE in a total lipid extract from ISOv treated sequentially with TNBS followed by DFDNB. (**H**) ISOv prepared from aztreonam-treated *E. coli* cells were subjected to SCAM analysis as in Fig. 2D to establish uniform inside out orientation. cps, counts per second.

PE and PS of sonicated dispersions react to completion within 1 hour with TNBS (fig. S7A). In detergent-solubilized ISOv prepared from EH150, 97% of PE and PS was derivatized with TNBS in 1 hour on ice (fig. S7, B and C). Therefore, under our conditions, all surface-exposed PE and PS would be derivatized consistent with 66 to 70% of PE and 96 to 98% of PS (from about 10% of total) localized to the lumen of ISOv (periplasmic leaflet).

To validate the sidedness assay conditions, we subjected a total extract of ISOv of EH150 (Fig. 4B) to normal-phase LC/MS/MS (liquid chromatography–tandem mass spectrometry) analysis (Fig. 4D). The percentage of derivatized TNP-PE and DNP-PE and TNP-PS and DNP-PS was calculated from mass spectra of analyzed species, which were ionized similarly. These results indicate that nearly 97% of the PS was represented by the dinitrophenylated form, indicating the predominant presence of PS within the lumenal surface (periplasmic side of cells) of the ISOv. This finding was unexpected since PS synthase is a cytoplasmically localized peripheral membrane protein (*10*), suggesting that PS is either made on periplasmic leaflet or translocated to the periplasmic leaflet immediately after synthesis. These results pose a provocative question as to the localization of the active site of PS decarboxylase or reciprocal lipid flip-flop for PS and PE. However, note that EH150 grown at the restrictive temperature is filamentous (*26*), which may explain the unexpected distribution of PE and PS (see the next section).

Transmembrane distribution of PE in IM of filamentous *E. coli* cells

Because of its relatively small head group, PE should prefer the concave volume of the inner leaflet of the lipid bilayer, supporting the idea that the asymmetric localization of PE membranes can stabilize a given morphology of cells or organelles (*27*). PE-lacking cells are filamentous (*28*). Therefore, to differentiate between cell morphology and PE levels as a determinant of PE localization, we analyzed transmembrane distribution of PE in wild-type *E. coli* cells containing 75% of PE but adapting a filamentous shape. Treatment of *E. coli* cells with the antibiotic aztreonam (*29*) induces cell filamentation and blocks cell division but still allows cell growth (Fig. 4E). ISOv prepared from filamentous *E. coli* were nearly 100% uniformly oriented (Fig. 4H). Aztreonam-treated cells contain around 60% of PE in their IM based on ^{32}P radiolabeling, as shown in fig. S5. Unexpectedly, we found that PE was predominantly found in the periplasmic leaflet of the IM of filamentous cells (Fig. 4, F and G), suggesting that PE is dynamically redistributed within the lipid bilayer either reflecting or facilitating a change in cell morphology. In a separate experiment, only 10% of total PE was labeled by TNBS in intact uniformly oriented ISOv isolated from aztreonam-treated cells (fig. S7, D and E), with the remaining 90% fully accessible to TNBS in the presence of detergent. Unlike for rod-shaped cells, no PE is inaccessible to TNBS on filamentous cells. Thus, these control experiments confirm the mirrored asymmetric distribution of PE in filamentous versus rod-shaped cells. Most of the PG is converted into CL when all PE was derivatized during incubation of ISOv from filamentous cells with TNBS, which was not observed with rod-shaped cells. Note that this enzymatic conversion does not require metabolic energy and readily occurs in stationary cells (*30*).

Transmembrane distribution of de novo synthesized PE in IM of initially filamentous *E. coli* lacking PE

To determine the sidedness of PE during its synthesis starting from cells beginning with near-zero amounts to wild-type levels, strain AT2033 was induced for de novo PE biosynthesis after growth under conditions in which PE was initially absent and cells were filamentous

(*31*). Cell aliquots were collected at the indicated times (Fig. 5) and converted to ISOv. PE derivatives were visualized after TLC analysis (Fig. 5A) and quantified by TLC elution–based analysis after sequential treatment of ISOv by TNBS followed by DFDNB (Fig. 5B). PE is initially enriched in the periplasmic leaflet of filamentous cells and progresses to near equal distribution and finally wild-type enrichment in the cytoplasmic leaflet as cells progressively adopt a rod shape and total PE increases from near zero to 75% of total membrane phospholipids (Fig. 5, A and B). Thus, transmembrane distribution of PE in rod-shaped and filamentous cells is inversely correlated.

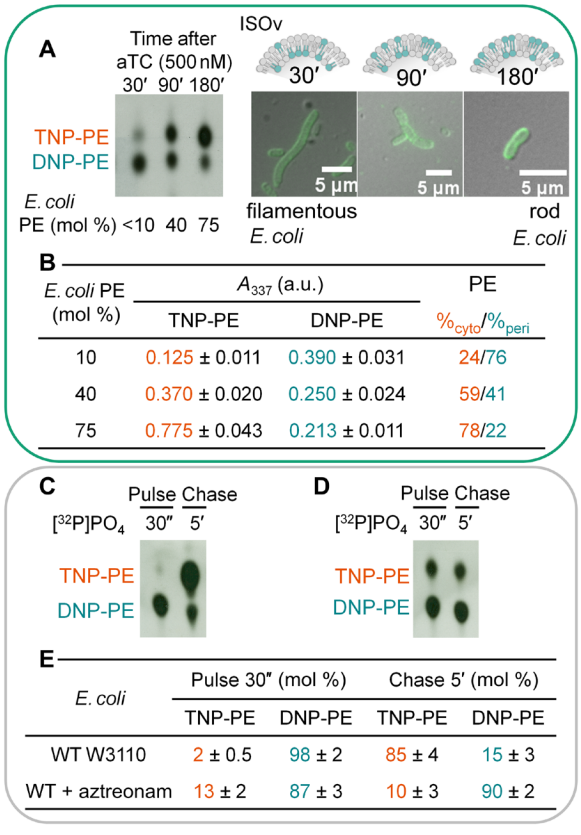

E. coli PE (mol %)	A_{337} (a.u.) TNP-PE	A_{337} (a.u.) DNP-PE	PE $\%_{cyto}/\%_{peri}$
10	0.125 ± 0.011	0.390 ± 0.031	24/76
40	0.370 ± 0.020	0.250 ± 0.024	59/41
75	0.775 ± 0.043	0.213 ± 0.011	78/22

E. coli	Pulse 30″ (mol %) TNP-PE	Pulse 30″ (mol %) DNP-PE	Chase 5′ (mol %) TNP-PE	Chase 5′ (mol %) DNP-PE
WT W3110	2 ± 0.5	98 ± 2	85 ± 4	15 ± 3
WT + aztreonam	13 ± 2	87 ± 3	10 ± 3	90 ± 2

Fig. 5. Transbilayer distribution of PE in the IM as a function of phospholipid composition and cell shape in ISOv prepared from initially filamentous *E. coli* strain AT2033 induced for PE biosynthesis. (**A**) Cell aliquots were collected at the indicated times after addition of inducer for PE synthesis and converted to ISOv. TLC with derivatized phospholipids from ISOv treated sequentially with TNBS followed by DFDNB is shown. Diagrams representing progressive PE enrichment of outer leaflet of ISOv corresponding topologically to the cytoplasmic side of the IM of cells progressively adopting a rod shape are shown. Microscope images of representative cells outgrown in the presence of anhydrotetracycline (aTC) for 30, 90, and 180 min. (**B**) Determined transbilayer distribution of PE. Total lipids were extracted from ISOv labeled sequentially with TNBS followed by DFDNB, and the amounts of eluted TNP-PE and DNP-PE derivatives were determined from the absorbance at 337 nm after elution from TLC. Values are average absorbances (±SD) from three experiments, where each determination was performed in duplicate. Variation between ratiometric estimations of transmembrane distribution was ±3% of the percent values. (**C** to **E**) Pulse-chase labeling analysis of newly synthesized PE in wild-type (WT) and filamentous *E. coli*. Movement of [^{32}P]PO_4 pulse-labeled PE from periplasmic leaflet accessible to DFDNB to cytoplasmic leaflet accessible to TNBS during a chase of radiolabel. (C) W3110 *E. coli* cells were labeled for 30 s, followed by 5-min chase of radiolabel, and converted to ISOv, which were sequentially treated with TNBS/DFDNB followed by TLC separation of products. (D) Pulse-chase labeling analysis of newly synthesized PE in filamentous *E. coli*. Cells pretreated with aztreonam before analysis as described in (C) above. Same as in (C) (30-s pulse) followed by 5-min chase of radiolabel. (E) Estimated distribution of pulse-labeled and pulse-chased PE derivatives from experiment (C) and (D). Values are averages (±SD) from two experiments, where each determination was performed in duplicate.

Dynamic distribution of newly synthesized PE

Enrichment of PE in the periplasmic leaflet of fully anionic membranes is consistent with enrichment of its precursor PS (Fig. 4, A to D). These results were obtained from systems at equilibrium. Experiments in filamentous cells (EH150, AT2033, and aztreonam-treated wild type) suggest that newly synthesized PS and PE may first populate the periplasmic leaflet of the IM. To see whether nascent PE first appears on the periplasmic side of the IM in wild-type rod-shaped cells followed by dynamic and disproportional distribution to the cytoplasmic leaflet, cells were labeled with [^{32}P]PO_4 for 30 s, followed by a chase for 5 min. Cells from both time points were converted into ISOv, which were labeled sequentially with TNBS followed by DFDNB. As shown in Fig. 5C, the nascent [^{32}P]PO_4-labeled PE is predominantly derivatized by permeable DFDNB into DNP-PE and scarcely present as the TNP-PE form at the cytoplasmic leaflet of ISOv prepared from cells labeled for 30 s. After the 5-min chase with excess unlabeled phosphate, the nascent PE first appearing in the periplasmic leaflet now appeared as the TNBS-derivatized form in the cytoplasmic leaflet, consistent with its retrograde dynamic movement to satisfy unique biosynthetic and topological constraints (Fig. 5C). These results pose again a provocative question as to the localization of the active site of PS decarboxylase and reciprocal lipid flip-flop of PS and PE.

To see whether nascent PE also first appears on the periplasmic side of the IM in aztreonam-treated wild-type filamentous cells followed by delayed disproportional distribution to the cytoplasmic leaflet, cells were labeled with [^{32}P]PO_4 for 30 s, chased for 5 min, and converted into ISOv, which were labeled sequentially with TNBS followed by DFDNB. As shown in Fig. 5E, the nascent PE is predominantly derivatized by permeable DFDNB in periplasmic leaflet of ISOv from cells labeled for 30 s. After the chase with unlabeled phosphate, the nascent PE first appearing in the periplasmic leaflet remains largely as the DFDNB-derivatized form in the periplasmic leaflet (Fig. 5D). Thus, its retrograde movement to the cytoplasmic leaflet is minimal based on the low level of derivatization by TNBS in the cytoplasmic leaflet of ISOv. These data are consistent with the higher amount of PE in the periplasmic leaflet of filamentous cells due to its apparent reduced retrograde movement to the cytoplasmic leaflet or continuous biosynthetic buildup at this leaflet. Thus, transmembrane asymmetry of PE could be maintained also by a metabolic mechanism, which relies on delicate balance of anabolic and catabolic reactions on both sides of the IM.

Establishment of putative link between asymmetry of PE and lipid order homeostasis in the IM

It was suggested that the inner leaflet is highly compressed during bacterial cell growth (*15*). Do cells balance distribution of lipids across the lipid bilayer to satisfy an intermolecular packing of lipids and their physical order in each membrane leaflet? To answer this question, we monitored lipid order using the NR12S fluorescent probe whose fluorescence emission is highly sensitive to the lipid order of the outer leaflet of membrane (*21*). Alternatively, a relatively new push-pull pyrene analogue (PA) probe was used as a control for monitoring

the lipid order in ISOv but without leaflet selectivity (*32*). Both probes undergo a shift toward shorter wavelengths in L_o phases as compared to L_d phases independent of membrane surface charge but sensitive to the hydration and rigidity of the microenvironment. Thus, we expected detection of different extents of the L_d phase within both leaflets of ISOv. The lipid order of outer leaflet of ISOv was progressively increased as the amount of PE was increased from zero [AL95 with no PE; containing 50 mole percent (mol %) CL (*31*)] to 75% of total membrane phospholipids (*E. coli* AT2033 + 100 and *E. coli* AL95/pDD72) and then to 95% (*E. coli* UE54) (*25*), as evidenced by the blue shift (Fig. 6A) in the fluorescence emission maximum and progressive increase in both the NR12S F_{560}/F_{610} (Fig. 6B) and push-pull pyrene PA F_{480}/F_{580} (Fig. 6D) intensity ratios. This ratio reaches maxima for ISOv made from *E. coli* UE54 and the triple *clsABC null E. coli* mutant BKT12 completely lacking both PG and CL or only CL, respectively. The highest red shift was observed for ISOv from AL95 (Fig. 6, A to D), which is followed by increased hydration of the heavily CL-enriched monolayer and forming a more disordered phase. Note that leaflet-specific NR12S did not detect a significant difference between the different PE amount in *E. coli* AT2033, while the leaflet-nonspecific PA probe showed a progressive increase in the lipid order in ISOv made from cells outgrown with anhydrotetracycline (aTC; 20, 50, and 100 ng/ml) (Fig. 6, C and D), demonstrating that gradual changes in lipid packing order take place predominantly in the luminal leaflet of ISOv (corresponding to periplasmic leaflet of IM) when amounts of PE and CL are redistributed

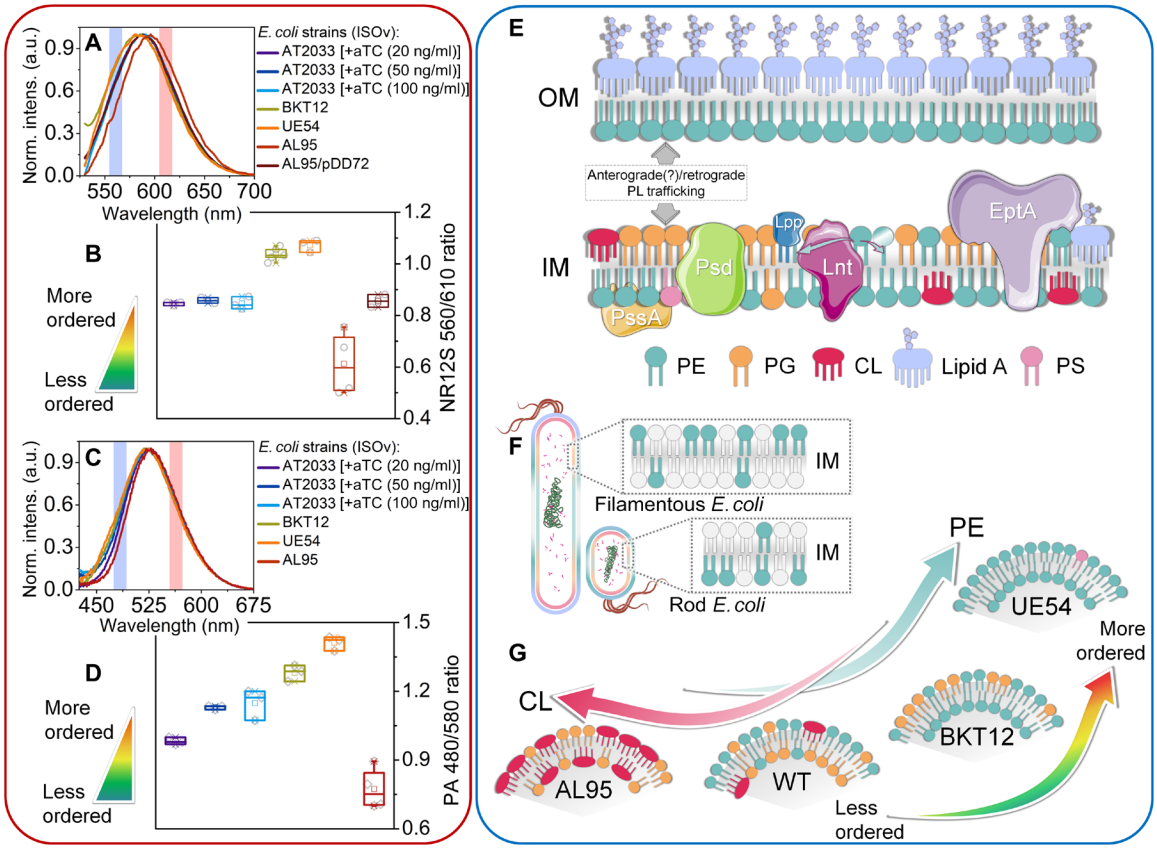

Fig. 6. Transbilayer distribution of PE and lipid order in the IM as a function of phospholipid composition in ISOv prepared from *E. coli* strains with different PE content. Normalized fluorescence spectra of 20 nM NR12S (**A**) and 100 nM push-pull pyrene PA (**C**) after treatment of ISOv with the probe. Strain AT2033 was outgrown with aTC (20, 50, or 100 ng/ml), resulting in different but uniform cell-to-cell PE content (*31*). Strain AL95 with or without plasmid pDD72 contains wild-type levels of PE or no PE, respectively. Strains BKT12 and UE54 are mutants that contain no CL or no CL and PG, respectively. Response of the NR12S probe [F_{560}/F_{610} ratio; (**B**)] and PA probe [F_{480}/F_{580} ratio; (**D**)] to in vivo modification of the lipid composition of IM ISOv. (**E**) Biogenic nature of lipid asymmetry in Gram-negative bacteria. Although compositional phospholipid asymmetry within the IM can be explained by sidedness of PE synthesis (by action of PS synthase and decarboxylase) or breakdown [by apolipoprotein *N*-acyltransferase (Lnt) on periplasmic surface of resting and, additionally, by lipid A phosphoethanolamine transferase (EptA) on periplasmic surface of stressed cells, respectively], it can rely also on transport of specific lipids between the IM and OM. The functioning of Mla (Maintenance of lipid asymmetry) FEDB machinery in an anterograde rather than a retrograde direction opens this possibility via continuous removal of lipids from the periplasmic leaflet by MlaD (*37*). All these processes can create lipid concentration gradients and downhill flows. Lnt transfers the fatty acid moiety from donor PE to the N terminus of a major OM lipoprotein precursor (Lpp), and releases a lysophosphatidylethanolamine as by-product. EptA, a phosphoethanolamine transferase, catalyzes continuous modification of newly synthesized lipid A core by adding a phosphoethanolamine moiety to lipid A in antibiotic- or cold-stressed cells. The LplT/Aas system [transporter (LplT) and acyltransferase-acyl carrier protein synthetase (Aas) phospholipid repair tandem system] is activated in stressed cells (and therefore is not shown) to facilitate a retrograde translocation across the IM and specific remodeling of all three major phospholipids. (**F**) Mirrored asymmetry of PE in filamentous and rod-shaped cells is shown (table S2). (**G**) An establishment of link between compositional and physical asymmetries. Disproportional progressive differences in amounts of PE and CL and lipid order are shown with different colored arrows. Since, in wild-type cells, PE is located primarily in the cytoplasmic leaflet of IM without fatty acyl group asymmetry (fig. S6), lipid rigidity in the two monolayers of the bilayer may be also asymmetrically distributed because of different content and/or disproportional distribution of PE and CL.

between two membrane leaflets. The observed difference in experiments with NR12S and PA probes can be due to differences in dynamic range of fluorescence of push-pull pyrene PA and NR12S probes (up to 100 and 50 nm, respectively). Thus, PA as a probe with enhanced dynamic range of fluorescence can be advantageous in the sensing of lipid packing order. These findings are consistent with the experiments on artificial membranes (fig. S8, A to D), which rule out the contribution of the bulk protein component to this phenomenon and favor an idea that the two lipids, PE and CL, may counteract each other to adjust the lipid order of the bilayer. The reciprocal tendency of PE to increase lipid order and the tendency of CL to decrease this order may be correlated with tight or looser intermolecular packing of lipids and/or differences in outer leaflet hydration levels.

DISCUSSION

The distribution of aminophospholipids (PE and PS) in the membranes of Gram-positive bacteria was known to be asymmetric from previous experiments using TNBS probe. PE distribution was 67%/33% and 80%/20% favoring the cytoplasmic leaflet of *Bacillus megaterium* (*12*, *15*) and eukaryotic cells (*22*), respectively. At the same time, the PE in *Bacillus amyloliquefaciens* was found to be located predominantly in the outer leaflet of cytoplasmic membrane (*33*). Although still controversial, these studies indicate that PE is asymmetrically distributed in bacterial membranes and raised the question of its transmembrane distribution in Gram-negative bacteria, which have a more complex envelope system of IMs and OMs. No similar investigations have been reported for Gram-negative bacteria. Thus, we exploited permeant and nonpermeant amino group–specific probes to determine the aminophospholipid head group distribution, followed by assessment of their acyl group asymmetries in the *E. coli* IM. Characterization of labeled lipids with independent radiolabeled, normal-phase LC/MS/MS, TLC elution–based, and TLC-less spectrophotometric assays allowed us to reveal asymmetrical, dynamic, and cell shape–dependent PE distribution in the IM of Gram-negative bacteria.

Our work represents a technical and conceptual breakthrough in the following areas:

1) Quantitative analysis of PE sidedness led to the first unambiguous demonstration of PE asymmetry in IM of Gram-negative bacteria such as *E. coli* (Figs. 2 and 3) and *Y. pseudotuberculosis* (fig. S4), which has long remained unknown.

2) Asymmetry of PE is a remarkable dynamic. PE appears first on the periplasmic side of the IM of *E. coli* cells, followed by dynamic and disproportional distribution to the cytoplasmic leaflet (Fig. 5).

3) Rod-shaped and filamentous *E. coli* cells display an opposite distribution of PE in their IMs (Figs. 3 and 4, E to H). This very intriguing finding suggests that PE distribution facilitates or results from changes in bacterial shape. The rates of de novo fatty acid and CL biosynthesis can dictate bacterial shape, as was demonstrated recently (*34*, *35*). The rate of CL biosynthesis and cells shape of logarithmically grown *E. coli* cells are interrelated quantitatively (*35*). Gradual changes in distribution of PE/CL amounts between the IM leaflets during de novo PE biosynthesis in *E. coli* cells initially lacking PE coincides with progressive reduction of cell size (Fig. 5A). PE is progressively accumulated, but CL is dissipated from the cytoplasmic leaflet of the IM. These transmembrane redistributions of CL and PE correlate with gradual changes in lipid packing order predominantly in the luminal leaflet of ISOv (corresponding to periplasmic leaflet of IM) (Fig. 6, C and D), demonstrating the possible coinvolvement of all these events in bacterial size control.

4) Lipid asymmetry is most likely metabolically controlled, regulated, and maintained in the IM of Gram-negative bacteria. The transmembrane distribution of PE and PS presumably reflects the relative rates of synthesis, translocation, and utilization of these aminophospholipids and their metabolic precursors. The asymmetric distribution of PE in IM can result from the balance between its translocation to the cytoplasmic leaflet, biosynthetic buildup on this leaflet, and loss from the periplasmic leaflet due to biosynthetical utilization and flow to the OM (illustrated in Fig. 6E). This balance is likely to be different in rod-shaped and filamentous cells because of different relative areas of IM and OM and different dynamics of membrane growth. This may explain the opposite asymmetric distribution of PE in the IM of rod-shaped and filamentous cells (Fig. 4 and fig. S7, D and E; illustrated in Fig. 6F).

5) At any given time, more and more PE molecules are required at the outer leaflet of IM to generate mature triacylated lipoprotein precursor (Lpp) and provide material for exclusive building of the PE-enriched periplasmic leaflet of the OM (Fig. 6E). This is consistent with initial appearance of nascent PE in the outer IM leaflet in all cell types examined (Fig. 5). Although it may be advantageous to have the precursor of PS initially present in the IM periplasmic leaflet, a puzzling aspect of PS localization and accumulation in this leaflet in the *psd* conditionally lethal mutant (Fig. 4, A to D, and fig. S7, B and C) can be explained by its inability to serve as an acyl donor in the reaction with mature Lpp catalyzed by apolipoprotein *N*-acyltransferase (Fig. 6E). Nevertheless these results pose a provocative question as to the localization of the active site of PS decarboxylase and necessitate anterograde and retrograde movement of PS and PE, respectively.

6) No changes in acyl group asymmetry of PE, PG, or PS were observed in the IM of wild-type *E. coli* and its lipid mutants (fig. S6). Our observations suggest rather an existence of a link between PE distribution, CL content, and lipid order within the IM. Since PE may increase the bilayer rigidity in the range comparable with that of cholesterol (*36*), our results suggest that bacteria may maintain membrane leaflet composition and the lipid order and rigidity not only by regulating the saturation state of the newly synthetized phospholipids, as widely accepted, but also by a fine-tuning of PE and CL content of individual leaflets. Thus, compositional asymmetries and physical order can be intrinsically coupled in bacterial membranes (Fig. 6, A to D, and fig. S8, A to D; illustrated in Fig. 6G).

Although membrane asymmetry is largely related to lipid distribution, a full understanding of the physiological significance and detailed molecular mechanisms by which membrane phospholipid asymmetry is generated and maintained is lacking. In this work, we report novel methodology for determination of aminophospholipid asymmetry, which is based on complementary labeling of their head groups by two vectorial chemical probes, TNBS and DFDNB. To determine both head group and acyl asymmetry, the labeled lipids could be further characterized to determine head group and acyl asymmetry of aminophospholipids using radiometric, mass spectrometric methods, and spectrophotometric approaches. These methods are suitable for investigation of transbilayer dynamics, steady-state sidedness, and physiological significance of aminolipid asymmetry in Gram-negative (PE, PS, and ornithine lipids) and Gram-positive (*O*-lysylphosphatidylglycerol) bacteria and in any single-membrane cellular organelle (exosomes and apoptotic bodies).

Our results reveal unexpected opposite asymmetry of PE in the cytoplasmic and periplasmic leaflets of *E. coli* IM of rod-shaped and filamentous cells. PE is dynamically redistributed within the IM either reflecting or facilitating the changes in cell shape. In eukaryotic cells, lipid asymmetry is maintained by the interplay of glycerophospholipid flippases and scramblases, which have not been discovered in bacterial cells. Thus, bacterial cells have to rely on different mechanisms for maintaining the membrane asymmetry. One of such mechanism is the dynamic balance between the incorporation of phospholipids into the cytoplasmic leaflet (due to their continuous synthesis) and their removal from the periplasmic leaflet (due to transport to the OM or usage in metabolic pathways involving periplasmic lipoproteins). This may create a steady-state concentration gradient of the lipids resulting in IM lipid asymmetry. Still unknown mechanisms of anterograde transport from IM to OM may accommodate the rates of de novo glycerophospholipid biosynthesis and dictate bacterial size, as was proposed recently (*37*). Thus, PE asymmetry in the IM might originate metabolically and play a central role in regulating the size and morphology of Gram-negative bacteria along with balanced synthesis of certain cell cycle proteins (*20*).

We also revealed that compositional asymmetries and physical order can be intrinsically coupled in the biogenic IM. The change in transmembrane distribution of two nonbilayer prone lipids, PE and CL, is tightly coupled to adjust the collective physical properties of the membrane. It is possible to speculate that this fundamental feature may be a main architectural principle for most, if not all, living biological membranes.

Obviously, further studies are necessary to fully elucidate the mechanisms and physiological consequences of our findings. Nevertheless, our results provide a conceptual basis and experimental tools for studying the transbilayer dynamics and regulatory function of various aminolipids (PE, PS, *O*-lysylphosphatidylglycerol, ornithine lipids, and some sphingolipids) in different organisms. These approaches offer the possibility of investigating the sidedness of aminolipids and establishment of their head and acyl group asymmetries in different single-membrane systems ranging from intact cell membranes of bacteria to erythrocytes, cell-derived organelles, and liposomes.

MATERIALS AND METHODS

Reagents

aTC was from Spectrum Chemical Manufacturing Corp. [^{32}P]PO4 was from PerkinElmer, MP Biomedicals, or American Radiolabeled Chemicals Inc. TNBS and DFDNB were purchased from Thermo Fisher Scientific and Sigma-Aldrich, respectively. MPB and AMS were purchased from Invitrogen Molecular Probes Biotechnology; *n*-OG and βME were purchased from Sigma-Aldrich. Carbonyl cyanide *m*-chlorophenyl hydrazine came from Sigma-Aldrich. *E. coli* polar lipid extract, *E. coli* CL, dipalmitoylphosphatidylethanolamine (DPPE), and dipalmitoylphosphatidylserine (DPPS) were purchased from Avanti Polar Lipids (Alabaster, AL). Streptavidin-conjugated Alexa Fluor 430, avidin–horseradish peroxidase, and SuperSignal West Pico chemiluminescent substrate came from Thermo Fisher Scientific. Aztreonam was obtained from Sigma-Aldrich. Biotinylated Ro09-0198 was a gift from M. Umeda (Kyoto University, Japan). Antibodies directed against SecA and PldA were gifts from K.-i. Nishiyama (Iwate University, Morioka, Japan) and J. Tommassen (Utrecht University, The Netherlands), respectively. NR12S and pyrene PA probes were gifts from A. Klymchenko (University of Strasbourg, France), O. Kucherak (Charles University, Prague), and Y. Niko (Kochi University, Japan).

Bacterial strains, cell growth, and regulated expression of the *pssA* gene

E. coli strains W3110 and W3899 are wild type with respect to glycerophospholipid biosynthesis and composition. UE54 (*lpp2 Δara714 rcsF*::mini-*Tn10$_{cam}$* Δ*pgsA*::FRT-*Kan*-FRT) carries a null allele of the *pgsA* gene encoding the committed step to PG and CL biosynthesis, making it devoid of PG and CL and containing, at stationery phase of growth, about 95 mol % of PE, 3 mol % of PA, and 2 mol % of cytidine 5′-diphosphate–diacylglycerol (*25*, *38*). These strains were grown on Luria-Bertani (LB) medium until reaching logarithmic phase of growth [OD_{600} (optical density at 600 nm) of 0.5 to 0.6]. EH150 [*psd-2(ts) purA*$^+$] carries a thermosensitive mutation in PS decarboxylase, which accumulates up to 70 mol % of PS in place of PE when grown in the presence of divalent cations. This strain was grown on LB medium supplemented with 25 mM $MgCl_2$ until reaching early logarithmic phase of growth (OD_{600} of 0.3) and then transferred to 42°C where growth was continued for another 3 hours. Strain AL95 (*pss93::kan lacY::Tn9*) lacks the ability to synthesize PE and therefore contains only acidic phospholipids PG and CL (45 and 50%, respectively) and phosphatidic acid (PA) which altogether makeup an IM consisting of only negatively charged phospholipids (*7*, *31*). This strain was grown in LB liquid medium supplemented with 50 mM $MgCl_2$, which is required for viability. Strain AT2033 (*P$_{LtetO-1}$-pssA+ pss93::kanR lacY::Tn9 recA srl::Tn10*) in which the PE content of the cell can be regulated from near-zero to wild-type level (75%) proportional to the amount of gene inducer aTC in the growth medium (*7*, *31*). Strain AT2033 was grown first overnight on LB medium supplemented with 50 mM $MgCl_2$ and then outgrown in the same medium until an OD_{600} of 0.5 to 0.6. Cultures were supplemented with 0.5 μM aTC and harvested after 10, 90, or 180 min of growth. Cells that were outgrown for 30 min with this amount of aTC in the presence of 50 mM $MgCl_2$ were filamentous, as expected, whereas cells outgrown for 180 min adopted a rod shape and exhibited uniform high green fluorescence (*7*, *31*) after being labeled with strictly PE-specific Ro09-0198 in the presence of EDTA. For preparation of [^{32}P]-labeled ISOv, cells were uniformly labeled with [^{32}P]PO_4 (1 μCi/ml) after dilution to A_{600} of 0.05 to initiate logarithmic growth, followed by growth until OD_{600} of 0.5 to 0.6. Filamentous cells were generated by growth in the presence of aztreonam (1 μg/ml) (*29*). *Y. pseudotuberculosis* serotype O:1b IP32953 was routinely grown at 28°C on LB medium.

Preparation of uniformly oriented and sealed ISOv

ISOv were prepared from *E. coli* wild-type cells, UE54, AT2033, and EH150 containing 75%, 95%, and varied amounts of PE or PS, respectively, as described previously by rupture of cells using a French press at 560 kg/cm^2 (8000 psi) with subsequent differential or isopycnic centrifugations (*6*). Vesicles were concentrated by centrifugation, resuspended in ice-cold 100 mM Hepes buffer (pH 8.1) containing 250 mM sucrose and 25 mM $MgCl_2$ at a protein concentration of 5 to 10 mg/ml, and stored at −80°C. Uniform orientation of ISOv was verified as previously described (*6*) based on the orientation of the essential protein LepB containing one reduced Cys residue exposed to the cytoplasm and two Cys residues in disulfide linkage exposed to the periplasm. SCAM uses a biotin-containing detectable (MPB; 10 μM) or nondetectable (AMS; 500 μM) membrane

impermeable thiol-reactive reagent to either label or preblock diagnostic reduced cysteines exposed to cytoplasmic side of the IM (*39*). ISOv were either labeled directly with MPB or first pretreated with AMS, followed by treatment with MPB in the presence or absence of OG or by MPB in the presence of OG and βME. All samples were solubilized with SDS subsequently inactivated by Lubrol-PX before immunoprecipitation with LepB-specific antibody, followed by SDS–polyacrylamide gel electrophoresis (SDS-PAGE) and Western blotting to detect biotinylated LepB (*39*). Labeling by MPB that can be blocked completely by pretreatment with AMS is an independent indication of an outward-facing residue, while the labeling by MPB that cannot be blocked by this AMS treatment is an independent indication of a residue that faces the lumen of ISOv. The percentage of IM vesicles that adapted ISO orientation was calculated from immunointensities of the LepB bands. Protein content of ISOv was determined with the BCA kit (Pierce). The absence of OM cross-contamination was verified by Western blotting with anti-SecA (IM) and anti-PldA (OM) antibodies.

Pulse-chase labeling analysis of newly synthesized PE

Logarithmically grown cells (100 ml) were labeled by incubation with carrier-free [^{32}P]PO_4 (10 μCi/ml) for 30 s, and radiolabel was chased for 5 min after addition of 1 mM nonradioactive phosphate. Pulse-labeled or chased cultures (100 ml) were harvested at corresponding time intervals and converted to ISOv as described above.

TLC analysis of lipids

^{32}P-labeled or nonradiolabeled phospholipids were resolved by TLC using HPTLC 60 silica gel plates (EMD, Gibbstown, NJ) impregnated for 1 min in 1.2% boric acid in ethanol-water (1:1) and activated and developed with solvent consisting of chloroform:methanol:water:ammonia (60:37.5:3:1, v/v) or chloroform:methanol:acetic acid (65:25:8, v/v), as described previously (*30*, *38*). The spots were assigned to different *E. coli* phospholipids, aminophospholipids, and their derivatives based on TLC mobility (Rf values) of in-house standards prepared by derivatization of synthetic or natural lipid (fig. S9). Identification of *N*-acylated PE (acyl-PE) (*N*-acyl-PE does not react with TNBS) was based on the presence or absence of corresponding spots in experiments involving steady-state or pulse labeling of viable lipid mutants containing or lacking PE, respectively, and mass spectrometric identification of TLC-resolved *N*-acyl-PE from *E. coli* UE54 (fig. S5). Nonradiolabeled lipids were quantified as described below. Radiolabeled lipids were visualized and quantified using a Personal Molecular Imager FX (Bio-Rad Laboratories). Stored images were processed and quantified using Quantity One software for scanning and analysis of the captured phosphor images (Bio-Rad Laboratories). Phospholipid content is expressed as mol % of total phospholipid (correcting for two phosphates per molecule of CL) based on the intensity of the captured signal on Phosphor screen generated by the radiolabeled spots on the TLC plate. The results presented are representative of three or more determinations.

Transmembrane distribution of PE in ISOv derived from reactions with permeant and nonpermeant primary amine–specific probes

The membrane nonpenetrating probe TNBS and the penetrating probe DFDNB were used to elucidate the aminophospholipid topography of *E. coli* IM. To determine the pool of PE that is accessible or protected in ISOv, 100 μl of ISOv with a protein concentration of 5 to 10 mg/ml was used routinely. For the derivatization of PE, TNBS or DFDNB was added either individually or first TNBS, followed by DFDNB, to give a final concentration of 1 and 5 mM, respectively. TNBS or DFDNB was always diluted 10-fold from a freshly prepared 5% stock solution in water or 100 mM stock solution in DMSO, respectively. The reaction was allowed proceeding with TNBS at 4°C and DFDNB at 37°C for 1 hour in the dark.

To determine the maximal pool of PE accessible to TNBS or DFDNB, samples were diluted before reaction with the labeling reagents in buffer containing OG at a final concentration of 40 or 5 mM, respectively. The labeling reaction was terminated by addition of an equal volume (100 μl) of 0.5 M NaCl in 0.1 M HCl, followed by 20 μl of 20% BSA or 5% of L-lysine. Lipids were extracted by first adding 0.6 ml of chloroform:methanol (1:2) to create a single-phase solution. After vigorous vortexing for 30 min, 200 μl of 0.5 M NaCl in 0.1 M HCl was added to convert the single-phase solution to a two-phase solution. After centrifugation at 20,800*g* for 5 min at room temperature, the lower phase was recovered and used for TLC, spectrophotometric, or LC/MS/MS analysis, as described below.

Transmembrane sidedness of PE in ^{32}P-labeled ISOv was determined from the proportion of underivatized PE and its trinitrophenylated derivatized product (TNP-PE) obtained after TNBS treatment of intact versus OG-solubilized ISOv (total amount of PE). Lipids after TLC separation were quantified as described above.

In the second assay, nonradiolabeled ISOv were treated separately by either TNBS or DFDNB or sequentially by TNBS followed by DFDNB. After extraction of lipids and separation by TLC, the plates were exposed to iodine to locate derivatized and nonderivatized PEs. TNP-PE and DNP-PE spots, representing PE from the outer and inner leaflets of the ISOv, respectively, were scraped from the TLC plates and the lipids eluted with the same extraction procedure used to extract the total lipids from ISOv. The absorbance of chloroform phase was recorded at 337 nm using a Shimadzu 1800 double-beam spectrophotometer.

In the third assay, the total amount of TNP-PE and DNP-PE in a lipid extract without TLC separation of lipids was determined by a spectrophotometric method. In this method, derivatization of PE was terminated by addition of 20 μl of 20% BSA or 5% L-lysine to inactivate residual TNBS and DFDNB. The scavenged amino-specific dyes remain at the interphase or in the aqueous phase during lipid extraction. The amount of PE in the outer and inner leaflets of the ISOv was determined in the total chloroform extract by measuring the absorbance of TNP-PE at 425 nm and DNP-PE at 375 nm. The A_{425}/A_{375} ratio was compared to standardized varied ratios of TNP-PE to DNP-PE to calculate the amount of each derivative. Absorbance spectra were recorded on Shimadzu 1800 or Varian 4000 ultraviolet-visible spectrophotometers. Alternatively, total lipid extract was subjected to normal-phase LC/MS/MS analysis.

Chemical modification of synthetic aminophospholipids in liposomes

Small unilamellar vesicles (SUVs) were prepared from DPPE or DPPS by sonication. Briefly, the stock solution of lipids in chloroform was dried in sample tubes to form a lipid film and then resuspended by sonication in 20 mM Na/Hepes buffer (pH 8.1) at a concentration of 2 μg/μl. TNBS or DFDNB was added to an aliquot of the SUVs to reach a final concentration of 1 mM. The mixture was incubated for 1 hour at 37°C. The reaction was stopped with an equal volume of

0.5 N NaCl in 0.1 N HCl solution. Phospholipids were extracted in chloroform/methanol, as described above and quantified on the basis of their respective absorbance.

Normal-phase LC/MS/MS analysis

Normal-phase LC was performed on an Agilent 1200 Quaternary LC system equipped with an Ascentis Silica HPLC column (5 µm, 25 cm by 2.1 mm; Sigma-Aldrich, St. Louis, MO). Mobile phase A consisted of chloroform/methanol/aqueous ammonium hydroxide (800:195:5, v/v). Mobile phase B consisted of chloroform/methanol/water/aqueous ammonium hydroxide (600:340:50:5, v/v). Mobile phase C consisted of chloroform/methanol/water/aqueous ammonium hydroxide (450:450:95:5, v/v). The elution program consisted of the following: 100% mobile phase A was held isocratically for 2 min, then linearly increased to 100% mobile phase B over 14 min, and held at 100% B for 11 min. The LC gradient was then changed to 100% mobile phase C for 3 min, held at 100% C for 3 min, and lastly returned to 100% A for 0.5 min and held at 100% A for 5 min. The LC eluent (with a total flow rate of 300 µl/min) was introduced into the electrospray ionization (ESI) source of a high-resolution TripleTOF 5600 mass spectrometer (SCIEX, Framingham, MA). Instrumental settings for negative ion ESI and MS/MS analysis of lipid species were as follows: IS = −4500 V, CUR = 20 psi, GSI = 20 psi, DP = −55 V, and FP = −150 V. The MS/MS analysis used nitrogen as the collision gas. Data analysis was performed using Analyst TF1.5 software (SCIEX, Framingham, MA).

Fluorescence microscopy and image processing

PE was detected in whole aztreonam-treated filamentous cells after conjugation with biotinylated Ro09-0198 in the presence of EDTA and detection by indirect fluorescence microscopy with streptavidin-conjugated Alexa Fluor 430, as described previously (*31*).

Fluorescent NR12S outer leaflet–specific lipid order and push-pull pyrene PA leaflet nonrestricted lipid order assays

ISOv were incubated with 20 nM NR12S or 100 nM PA (DMSO, <0.25%), respectively, at room temperature for 30 min. SUVs were incubated with 100 nM NR12S or 100 nM PA (DMSO, <0.25%) at room temperature for 15 min. Fluorescence spectra were recorded with a spectrofluorometer PTI QuantaMaster 40 using an excitation wavelength of 520 or 405 nm for each probe, respectively. To quantify the data, the F_{560}/F_{610} (NR12S) or F_{480}/F_{580} (push-pull pyrene PA) intensity ratio was calculated, where the higher values correspond to more ordered state within the membranes of ISOv or SUVs (*21*, *32*).

Numerical simulations

The methodology of quantum chemistry and molecular dynamics simulations used to elucidate the mechanism of prevalent mono-substituted DNP-PE formation is reported in section S1.

Scheme preparation

The combined figures from Servier Medical Art by Servier (licensed under a creative commons attribution 3.0 unported license) and KP were used.

Statistical analysis

The results of quantitative experiments are shown as means for independent experiments performed multiple times as indicated. Values are means (±SD) from three experiments, where each determination was performed in duplicate. Variation between duplicates was ±3%. Images represent three independent experiments.

SUPPLEMENTARY MATERIALS

Supplementary material for this article is available at http://advances.sciencemag.org/cgi/content/full/6/23/eaaz6333/DC1

View/request a protocol for this paper from *Bio-protocol*.

REFERENCES AND NOTES

1. D. Marquardt, B. Geier, G. Pabst, Asymmetric lipid membranes: Towards more realistic model systems. *Membranes* **5**, 180–196 (2015).
2. K. Emoto, T. Kobayashi, A. Yamaji, H. Aizawa, I. Yahara, K. Inoue, M. Umeda, Redistribution of phosphatidylethanolamine at the cleavage furrow of dividing cells during cytokinesis. *Proc. Natl. Acad. Sci. U.S.A.* **93**, 12867–12872 (1996).
3. J. H. Stafford, P. E. Thorpe, Increased exposure of phosphatidylethanolamine on the surface of tumor vascular endothelium. *Neoplasia* **13**, 299–308 (2011).
4. S. Furse, D. J. Scott, Three-dimensional distribution of phospholipids in Gram negative bacteria. *Biochemistry* **55**, 4742–4747 (2016).
5. M. Bogdanov, J. Sun, H. R. Kaback, W. Dowhan, A phospholipid acts as a chaperone in assembly of a membrane transport protein. *J. Biol. Chem.* **271**, 11615–11618 (1996).
6. M. Bogdanov, P. N. Heacock, W. Dowhan, A polytopic membrane protein displays a reversible topology dependent on membrane lipid composition. *EMBO J.* **21**, 2107–2116 (2002).
7. M. Bogdanov, J. Xie, P. Heacock, W. Dowhan, To flip or not to flip: Lipid-protein charge interactions are a determinant of final membrane protein topology. *J. Cell Biol.* **182**, 925–935 (2008).
8. E. Calzada, E. Avery, P. N. Sam, A. Modak, C. Wang, J. M. McCaffery, X. Han, N. N. Alder, S. M. Claypool, Phosphatidylethanolamine made in the inner mitochondrial membrane is essential for yeast cytochrome bc1 complex function. *Nat. Commun.* **10**, 1432 (2019).
9. C. Rathmann, A. S. Schlösser, J. Schiller, M. Bogdanov, T. Brüser, Tat transport in Escherichia coli requires zwitterionic phosphatidylethanolamine but no specific negatively charged phospholipid. *FEBS Lett.* **591**, 2848–2858 (2017).
10. K. Langley, E. Hawrot, E. Kennedy, Membrane assembly: Movement of phosphatidylserine between the cytoplasmic and outer membranes of Escherichia coli. *J. Bacteriol.* **152**, 1033–1041 (1982).
11. M. Murate, T. Kobayashi, Revisiting transbilayer distribution of lipids in the plasma membrane. *Chem. Phys. Lipids* **194**, 58–71 (2016).
12. J. E. Rothman, E. P. Kennedy, Asymmetrical distribution of phospholipids in the membrane of Bacillus megaterium. *J. Mol. Biol.* **110**, 603–618 (1977).
13. B. Eicher, D. Marquardt, F. A. Heberle, I. Letofsky-Papst, G. N. Rechberger, M.-S. Appavou, J. Katsaras, G. Pabst, Intrinsic curvature-mediated transbilayer coupling in asymmetric lipid vesicles. *Biophys. J.* **114**, 146–157 (2018).
14. J. C. Henderson, S. M. Zimmerman, A. A. Crofts, J. M. Boll, L. G. Kuhns, C. M. Herrera, M. S. Trent, The power of asymmetry: Architecture and assembly of the Gram-negative outer membrane lipid bilayer. *Annu. Rev. Microbiol.* **70**, 255–278 (2016).
15. J. E. Rothman, E. P. Kennedy, Rapid transmembrane movement of newly synthesized phospholipids during membrane assembly. *Proc. Natl. Acad. Sci. U.S.A.* **74**, 1821–1825 (1977).
16. S. E. Gordesky, G. V. Marinetti, The asymmetric arrangement of phospholipids in the human erythrocyte membrane. *Biochem. Biophys. Res. Commun.* **50**, 1027–1031 (1973).
17. J. A. Higgins, C. A. Pigott, Asymmetric distribution of phosphatidylethanolamine in the endoplasmic reticulum demonstrated using trinitrobenzenesulphonic acid as a probe. *Biochim. Biophys. Acta Biomembr.* **693**, 151–158 (1982).
18. G. Marinetti, R. Love, Differential reaction of cell membrane phospholipids and proteins with chemical probes. *Chem. Phys. Lipids* **16**, 239–254 (1976).
19. G. V. Marinetti, R. Love, Interaction of membrane aminophospholipids of E. coli with fluorodinitrobenzene and trinitrobenzenesulfonate. *Chem. Phys. Lipids* **18**, 170–180 (1977).
20. F. Si, G. Le Treut, J. T. Sauls, S. Vadia, P. A. Levin, S. Jun, Mechanistic origin of cell-size control and homeostasis in bacteria. *Curr. Biol.* **29**, 1760–1770.e7 (2019).
21. O. A. Kucherak, S. Oncul, Z. Darwich, D. A. Yushchenko, Y. Arntz, P. Didier, Y. Mely, A. S. Klymchenko, Switchable Nile Red-based probe for cholesterol and lipid order at the outer leaflet of biomembranes. *J. Am. Chem. Soc.* **132**, 4907–4916 (2010).
22. C. Valtersson, G. Dallner, Compartmentalization of phosphatidylethanolamine in microsomal membranes from rat liver. *J. Lipid Res.* **23**, 868–876 (1982).
23. S. P. Marfey, K. H. Tsai, Cross-linking of phospholipids in human erythrocyte membrane. *Biochem. Biophys. Res. Commun.* **65**, 31–38 (1975).
24. F. Hullin, H. Kim, N. Salem Jr., Analysis of aminophospholipid molecular species by high performance liquid chromatography. *J. Lipid Res.* **30**, 1963–1975 (1989).
25. Y. Shiba, Y. Yokoyama, Y. Aono, T. Kiuchi, J. Kusaka, K. Matsumoto, H. Hara, Activation of the Rcs signal transduction system is responsible for the thermosensitive growth defect of an *Escherichia coli* mutant lacking phosphatidylglycerol and cardiolipin. *J. Bacteriol.* **186**, 6526–6535 (2004).

26. E. Hawrot, E. P. Kennedy, Phospholipid composition and membrane function in phosphatidylserine decarboxylase mutants of *Escherichia coli*. *J. Biol. Chem.* **253**, 8213–8220 (1978).
27. A. Irie, K. Yamamoto, Y. Miki, M. Murakami, Phosphatidylethanolamine dynamics are required for osteoclast fusion. *Sci. Rep.* **7**, 46715 (2017).
28. A. DeChavigny, P. N. Heacock, W. Dowhan, Phosphatidylethanolamine may not be essential for the viability of *Escherichia coli*. *J. Biol. Chem.* **266**, 5323–5332 (1991).
29. S. R. Arends, D. S. Weiss, Inhibiting cell division in Escherichia coli has little if any effect on gene expression. *J. Bacteriol.* **186**, 880–884 (2004).
30. B. K. Tan, M. Bogdanov, J. Zhao, W. Dowhan, C. R. Raetz, Z. Guan, Discovery of a cardiolipin synthase utilizing phosphatidylethanolamine and phosphatidylglycerol as substrates. *Proc. Natl. Acad. Sci. U.S.A.* **109**, 16504–16509 (2012).
31. M. Bogdanov, W. Dowhan, Lipid-dependent generation of a dual topology for a membrane protein. *J. Biol. Chem.* **287**, 37939–37948 (2012).
32. Y. Niko, P. Didier, Y. Mely, G.-i. Konishi, A. S. Klymchenko, Bright and photostable push-pull pyrene dye visualizes lipid order variation between plasma and intracellular membranes. *Sci. Rep.* **6**, 18870 (2016).
33. J. Paton, B. May, W. Elliott, Membrane phospholipid asymmetry in Bacillus amyloliquefaciens. *J. Bacteriol.* **135**, 393–401 (1978).
34. S. Vadia, L. T. Jessica, R. Lucena, Z. Yang, D. R. Kellogg, J. D. Wang, P. A. Levin, Fatty acid availability sets cell envelope capacity and dictates microbial cell size. *Curr. Biol.* **27**, 1757–1767.e5 (2017).
35. Z. Zhang, Q. Zhang, S. Guan, H. Shi, Quantitative connection between cell size and growth rate by phospholipid metabolism. *Cells* **9**, 391 (2020).
36. R. Dawaliby, C. Trubbia, C. Delporte, C. Noyon, J.-M. Ruysschaert, P. Van Antwerpen, C. Govaerts, Phosphatidylethanolamine is a key regulator of membrane fluidity in eukaryotic cells. *J. Biol. Chem.* **291**, 3658–3667 (2016).
37. M. J. Powers, M. S. Trent, Intermembrane transport: Glycerophospholipid homeostasis of the Gram-negative cell envelope. *Proc. Natl. Acad. Sci. U.S.A.* **116**, 17147–17155 (2019).
38. Y. Lin, L. Zheng, M. Bogdanov, Measurement of lysophospholipid transport across the membrane using *Escherichia coli* spheroplasts, in *Intracellular Lipid Transport* (Springer, 2019), pp. 165–180.
39. M. Bogdanov, Mapping of membrane protein topology by Substituted Cysteine Accessibility Method (SCAM™), in *Bacterial Protein Secretion Systems: Methods and Protocols* (Humana Press, 2017), pp. 105–128.
40. M. J. Abraham, T. Murtola, R. Schulz, S. Páll, J. C. Smith, B. Hess, E. Lindahl, GROMACS: High performance molecular simulations through multi-level parallelism from laptops to supercomputers. *SoftwareX* **1–2**, 19–25 (2015).
41. S. O. Yesylevskyy, Pteros 2.0: Evolution of the fast parallel molecular analysis library for C++ and Python. *J. Comput. Chem.* **36**, 1480–1488 (2015).

Acknowledgments: We dedicate this work in memory of Eugene Kennedy and Chris Raetz whose extensively cited work on lipid metabolism and membrane structure and function are a great source of inspiration and innovation in membrane and lipid biology. We would like to acknowledge K.-i. Nishiyama (Iwate University, Morioka, Japan) and J. Tommassen (Utrecht University, The Netherlands) for the gift of antibodies directed against SecA and PldA, respectively; M. Umeda (Kyoto University, Japan) for the gift of biotinylated Ro09-0198; A. Klymchenko (University of Strasbourg, France), O. Kucherak (Charles University, Prague), and Y. Niko (Kochi University, Japan) for the gift of fluorescent probes NR12S and push-pull pyrene PA. We thank J. Spudich and V. Berka for thoughtful suggestions during preparation of the manuscript and development of spectrophotometric TLC-less PE sidedness assay, respectively. **Funding:** This work was supported by NATO Science for Peace and Security Programme SPS 985291 (to M.B.), the European Union's Horizon 2020 research and innovation programme under the Marie Skłodowska-Curie grant agreement nos. 690853 (to M.B., S.Y., and C.R.) and 796245 (to S.Y.), Program of Competitive Growth of Kazan Federal University (to M.B. and R.K.), Russian Science Foundation Grant RCF 20-14-00166 (to R.K.), National Institutes of General Medical Sciences Grant GM121493, and the John S. Dunn Foundation (to W.D.). K.P. is a recipient of a scholarship from the U.S. Fulbright Foundation (IIE Grantee ID E0579608) under the supervision of M.B. S.Y. and K.P. were also supported by a stipend from NATO Science for Peace and Security Programme-SPS 985291. **Author contributions:** M.B. developed the concept and experimental rationale and designed and performed the main experiments. K.P. performed experiments dedicated to the development of TLC-free PE sidedness spectrophotometric assays and lipid order analysis of individual membrane leaflets, contributed to the design of the figures, and assisted in TLC-based PE and PS sidedness assays. S.R. assisted in the development of PE sidedness assay with radiolabeled ISOv. V.B. and P.I. contributed to the development of spectrophotometric TLC-based PE sidedness assay. Z.G. performed LC-ESI MS of derivatized PEs. W.D. and R.K. were involved in the design of TLC-less sidedness and pulse-labeling assays. S.Y. performed ab initio quantum chemistry calculations and molecular dynamics simulations. C.R. designed quantum chemistry calculations and took part in their analysis. M.B. conceived, supervised, and administered the project and wrote the manuscript with contributions from W.D., K.P., and S.Y. All authors contributed to data analysis and interpretation of results. All authors reviewed the results and approved the final version of the manuscript. **Competing interests:** The authors declare that they have no competing interest. **Data and materials availability:** All data needed to evaluate the conclusions in the paper are present in the paper and/or the Supplementary Materials. Additional data related to this paper may be requested from the authors. Bacterial strains and plasmids can be provided by completed material transfer agreement.

Submitted 13 October 2019
Accepted 23 March 2020
Published 3 June 2020
10.1126/sciadv.aaz6333

Citation: M. Bogdanov, K. Pyrshev, S. Yesylevskyy, S. Ryabichko, V. Boiko, P. Ivanchenko, R. Kiyamova, Z. Guan, C. Ramseyer, W. Dowhan, Phospholipid distribution in the cytoplasmic membrane of Gram-negative bacteria is highly asymmetric, dynamic, and cell shape-dependent. *Sci. Adv.* **6**, eaaz6333 (2020).

ScienceAdvances

Phospholipid distribution in the cytoplasmic membrane of Gram-negative bacteria is highly asymmetric, dynamic, and cell shape-dependent

Mikhail Bogdanov, Kyrylo Pyrshev, Semen Yesylevskyy, Sergey Ryabichko, Vitalii Boiko, Pavlo Ivanchenko, Ramziya Kiyamova, Ziqiang Guan, Christophe Ramseyer and William Dowhan

Sci Adv **6** (23), eaaz6333.
DOI: 10.1126/sciadv.aaz6333